Materials Transactions, JIM, Vol. 39, No. 5 (1998), pp. 562 to 569

MEM Analysis on Electron Density Distribution of Superconductors, $Pb_2Sr_2Y_{0.90}Sr_{0.10}Cu_3O_8$, $Pb_2Sr_2Y_{1-x}Ca_xCu_3O_8$ ($x=0.25$ and 0.41) and $Pb_2Sr_2Ho_{0.64}Ca_{0.36}Cu_3O_8$

Yasuhiro Ono, Akihiro Bungo†, Takashi Noji, Yoji Koike and Tsuyoshi Kajitani

Department of Applied Physics, Graduate School of Engineering, Tohoku University, Sendai 980-8579, Japan

Detailed crystal structures of high-T_c superconductors $Pb_2Sr_2Y_{0.90}Sr_{0.10}Cu_3O_8$, $Pb_2Sr_2Y_{1-x}Ca_xCu_3O_8$ ($x=0.25$ and 0.41) and $Pb_2Sr_2Ho_{0.64}Ca_{0.36}Cu_3O_8$ were successfully determined by means of single crystal X-ray diffraction at room temperature. Space symmetry changes from C2/m ($x=0.10$ and 0.25) to Cmmm ($x=0.36$ and 0.41) with increasing divalent cation concentration, x. Their electron density distributions are determined by means of the maximum entropy method (MEM). Two- or four-splitting oxygen peaks clearly appear in the electron density maps of PbO plane, which is consistent with oxygen disorder models introduced to the present structure determination. In the electron density maps of monovalent copper plane, no peak corresponding to excess oxygens was observed at the 1×10^3 e/nm^3 contour level. In the vicinities of divalent copper in the conducting plane, some anomalous electron density distribution is represented in the yttrium compounds.

(Received November 19, 1997; In Final Form January 28, 1998)

Keywords: *high-T_c superconductor, $Pb_2Sr_2Ln_{1-x}Ca_xCu_3O_8$, X-ray diffraction, electron density distribution, maximum entropy method (MEM)*

I. Introduction

Since Cava *et al.*[1] discovered the 3212-type lead cuprate superconductor with $T_c \sim 70$ K, $Pb_2Sr_2(Y, Ca)Cu_3O_8$, a considerable number of studies have been made on a peculiar crystal structure of this superconductor by means of X-ray diffraction[1]-[5], neutron diffraction[6]-[9] and electron microscopy[10][11]. This layered compound consists of SrO-PbO-Cu-PbO-SrO "blocking" layer and double CuO_2 planes, interleaved by a Y^{3+} layer partly substituted with Ca^{2+}. There are two kinds of coppers, namely, Cu^{1+} and Cu^{2+} as in the case of non-superconducting $YBa_2Cu_3O_6$, where Cu^{1+} ion is in the oxygen-free layer and Cu^{2+} ion is situated in a pyramidal CuO_5 coordination. In the present system, the electron holes are doped to the conducting CuO_2 planes through partial substitution of Ca^{2+} for Y^{3+} in the range up to 50%[1]. Several space groups were assigned to this compound with different Ca-concentrations in the literature, *e.g.*, Cmmm (No. 65), orthorhombic, for $Pb_2Sr_2YCu_3O_8$[6], Pman (No. 62), orthorhombic, for $Pb_2Sr_2Y_{0.73}Ca_{0.27}Cu_3O_8$[7] and P4/mmm (No. 123), tetragonal, for $Pb_2Sr_2Y_{0.75}Ca_{0.25}Cu_3O_8$[2]. Those crystal structures have almost identical atomic arrangements except for disordered oxygens in the PbO planes. Correct crystal symmetry is still in controversy, but it is not the purpose of this work to determine which is the correct one relative to the other.

Visualization of the electron density distribution is important to get some hints on the origin of the charge transfer mechanism in the 3212-type superconductors. Collins[12] demonstrated the reconstruction procedure of the electron density map by means of the maximum entropy method (MEM) using imperfect single crystal X-ray diffraction data. Sakata *et al.*[13][14] modified Collins's formalism and obtained the electron density distributions of the rutile, TiO_2, and the ceria, CeO_2, from powder X-ray diffraction data. In the case of a complex compound, it is necessary to measure a large number of Bragg intensity data up to higher miller indeces for the reasonably accurate electron density distribution. However, in the powder diffraction, the reliable intensity data are relatively few and the overlapping of diffraction peaks is a serious problem at a high diffraction angle. If the powder sample contains impurity, the peak separation procedure becomes more complicated. In addition, the layered oxide superconductors, sometimes, do not give proper powder diffraction patterns due to the strong residual stresses introduced during the sample preparation. Those indicate that single crystal diffraction measurements, rather than powder diffraction, are believed to be better for the present study. The aim of this study is to determine the electron density distribution of the 3212-type lead cuprate superconductors by means of a combination of the MEM and conventional single crystal X-ray diffraction analysis.

† Present address: Microelectronics Research Laboratories, Mitsubishi Materials Corporation, 2270, Yokoze, Chichibu, Saitama 368, Japan.

II. Experimental

1. Single crystal growth and X-ray diffraction

Powder materials with nominal compositions, $Pb_2Sr_2YCu_3O_8$, $Pb_2Sr_2Y_{0.75}Ca_{0.25}Cu_3O_8$, $Pb_2Sr_2Y_{0.5}Ca_{0.5}Cu_3O_8$ and $Pb_2Sr_2Ho_{0.5}Ca_{0.5}Cu_3O_8$ were prepared by a two-step solid state reaction technique as described in Ref. (15). Single crystals, #1, #2, #3 and #4, were grown from the melts of target powder samples and PbO/NaCl flux (PbO:NaCl=7:17) in the 99% N_2 and 1% O_2 atmosphere. Grown crystals were annealed in a pure N_2 gas flow at 475°C for 100 h, which is effective in obtaining the superconductivity of the lead cuprates. Details of the single crystal growth were reported elsewhere[16]. The superconducting critical temperature T_c (mid-point) was determined by a standard DC four-point probe method in the temperature range from 4.2 to 300 K[17].

Single crystal X-ray diffraction measurement was carried out using RIGAKU AFC-5 and AFC-6 four-circle diffractometers with monochromatic MoKα radiation. Plate-like samples having typical dimmensions of $0.1\times0.1\times0.05$ mm^3 were cut from the single crystals. It was indicated that the samples have cleavage planes perpendicular to the [110], [1$\bar{1}$0] and [001] directions. Lattice parameters were obtained from 24 Bragg reflections selected at about $2\theta=30°$. The crystals #3 and #4 have an orthorhombic unit cell, but small monoclinic distortion ($\beta>90°$) was detected for crystals #1 and #2. Bragg intensities were carefully measured by the ω scan method in the range of $3°\leqq2\theta<30°$ and by the 2θ-ω scan in $2\theta\geqq30°$. The superconducting critical temperature, T_c, lattice parameters, mechanical set-ups of the diffractometers, measured area (octants), number of independent reflections, the divalent cation concentrations, x, of the $Pb_2Sr_2Ln_{1-x}M_xCu_3O_8$ single crystals and residuals (R-factors) are given in Table 1. The valency of each cation is estimated from the determined structure parameters based on the bond valence sum rule.

Table 1 Superconducting critical temperature, T_c, lattice parameters, mechanical set-ups of the diffractometers, measured area (octants), number of independent reflections, the divalent cation concentration of $Pb_2Sr_2Ln_{1-x}M_xCu_3O_8$ single crystals and residuals (R-factors).

Crystal	#1	#2	#3	#4
(Ln, M)	(Y, Sr)	(Y, Ca)	(Y, Ca)	(Ho, Ca)
T_c (K)	16.0	64.8	75.5	78.8
lattice parameters				
a (nm)	0.53909(17)	0.53814(9)	0.53965(17)	0.53855(14)
b (nm)	0.54310(11)	0.54216(9)	0.53992(15)	0.53951(13)
c (nm)	1.57345(69)	1.57349(52)	1.57767(25)	1.57538(37)
β (°)	90.13(4)	90.28(3)		
diffractometer	RIGAKU AFC-6		RIGAKU AFC-5	
radiation	MoKα (λ=0.71073)		MoKα (λ=0.71073)	
monochromator	PG (002)		PG (002)	
space group	C2/m (No. 12)		Cmmm (No. 65)	
2θ range (°)	3–80		3–90	
octants (hkl)	$+\pm\pm$		$+\pm\pm$	
number of independent reflections	742	955	598	670
x	0.10(6)	0.25(1)	0.41(2)	0.364(8)
R_F	0.063	0.060	0.069	0.058
R_{wF}	0.067	0.064	0.077	0.067

2. Maximum entropy method (MEM)

The electron density maps are successively obtained by an iterative calculation in the MEM. The electron density at the position $\boldsymbol{r}$, $\rho(\boldsymbol{r})$, is calculated from the prior electron density $\tau(\boldsymbol{r})$ in the newest iteration cycle. To obtain the most reliable $\rho(\boldsymbol{r})$, the entropy of information must be maximized under the constraint. The entropy of information is defined as

$$S=-\sum_{\boldsymbol{r}}\rho'(\boldsymbol{r})\ln[\rho'(\boldsymbol{r})/\tau'(\boldsymbol{r})], \tag{1}$$

where $\rho'(\boldsymbol{r})$ and $\tau'(\boldsymbol{r})$ are the normalized electron densities such as,

$$\rho'(\boldsymbol{r})=\rho(\boldsymbol{r})/\sum_{\boldsymbol{r}}\rho(\boldsymbol{r}) \tag{2}$$

$$\tau'(\boldsymbol{r})=\tau(\boldsymbol{r})/\sum_{\boldsymbol{r}}\tau(\boldsymbol{r}). \tag{3}$$

Using Lagrange multiplier λ, the constrained entropy, *i.e.*, a Lagrange function $Q(\lambda)$, is defined as

$$Q(\lambda)=S-(\lambda/2)C. \tag{4}$$

S and C are the entropy and constraint function, respectively. C is defined by summation:

$$C=N^{-1}\sum_{\boldsymbol{k}}|F_{cal}(\boldsymbol{k})-F_{obs}(\boldsymbol{k})|^2/\sigma^2(\boldsymbol{k}). \tag{5}$$

N is the number of observed structure factors, $F_{obs}(\boldsymbol{k})$, and $\sigma(\boldsymbol{k})$ is a standard deviation of $F_{obs}(\boldsymbol{k})$. $F_{cal}(\boldsymbol{k})$ is the calculated structure factor given as

$$F_{calc}(\boldsymbol{k})=\int\rho(\boldsymbol{r})\exp(-2\pi i\boldsymbol{k}\cdot\boldsymbol{r})\,dv. \tag{6}$$

The constraint function can be chosen in several different ways[12]-[14][18][19]. But the present calculation is carried out assuming a single "weak" constraint function after Collins[12] and Sakata[13][14].

Maximization of $Q(\lambda)$ can be accomplished under the condition of

$$\partial Q(\lambda)/\partial\rho(\boldsymbol{r})=0. \tag{7}$$

The $\rho(\boldsymbol{r})$ is calculated under the above condition as

$$\rho(\boldsymbol{r})=\exp\left[\ln\tau(\boldsymbol{r})+\lambda F_{cal}(0)N^{-1}\sum_{\boldsymbol{k}}\sigma^{-2}(\boldsymbol{k})\{F_{obs}(\boldsymbol{k})-F_{cal}(\boldsymbol{k})\}\exp(-2\pi i\boldsymbol{k}\cdot\boldsymbol{r})\right]. \tag{8}$$

Iterative calculation starts from the uniform electron density distribution[13][14][19] with the given λ values (0.01–0.2) and is continued until the convergence criterion, $C\leqq1$, is attained. We assembled the computer program, PEDAX-MEM (Precise Electron Density Analysis for X-ray diffraction data by MEM), based on the above eq. (8). In order to test this program, we calculated the electron

density distribution using the measured structure factors of the rutile, TiO_2, given by Sakata *et al.*[13] and confirmed that the obtained electron density maps are in very good agreement with those in their paper.

III. Results

1. Crystal structure determination

The Ca-free crystal #1 exhibits the superconductivity below $T_c=16.0$ K (Table 1), which is presumably due to the carrier doped with the partial substitution of Sr^{2+} for Y^{3+}. Due to the very small difference in the atomic scattering factors of Y^{3+} and Sr^{2+}, being identical at the scattering vector, $k=0$, we could merely evaluate Sr-concentration of crystal #1 from a linear relation between the *c*-axis length and the mean ionic radius of an atom situated at the Ln site, r_{mean}. The value of r_{mean} was calculated assuming a linear law, $r_{mean}=r_{Ln}\times(1-x)+r_M\times x$, where r_{Ln} and r_M are the ionic rudii of lanthanide and divalent cation[20], respectively, and x is the site occupation probability of the divalent cation.

Figure 1 shows the *c*-axis length of the present samples, #2, #3 and #4. The abscissa is the calculated mean ionic radius, r_{mean}. The site occupancy, x, was determined by the standard structural analysis described in the following. A straight solid line in Fig. 1 was obtained by a least-square fitting to the three data points. The *c*-axis length of sample #1 corresponds to $r_{mean}=0.1044(59)$ nm in the straight line. The Sr-concentration of crystal #1 was thus determined to be $x=0.10(6)$.

Xue *et al.*[21] successfully determined the crystal structures of several Ca-free 3212-type compounds, $Pb_2Sr_2LnCu_3O_8$ (Ln=Nd, Tb and Pr) with space groups C2/m (No. 12), $Pb_2Sr_2LaCu_3O_8$ with Cmmm (No. 65) and $Pb_2Sr_2LnCu_3O_8$ (Ln=Eu and Dy) with P4/mmm (No. 123), by means of single crystal X-ray diffraction. We tentatively assigned the space group C2/m to the crystals #1 and #2, and Cmmm to #3 and #4, respectively. Weak Bragg reflections violating C-centering condition, *i.e.*, $h+k=2n+1$ where n is an integer number, were omitted from the intensity data sets for the present structure determination. Such reflections may occur from $\lambda/2$ component of Mo radiation. The mass absorption effect of the plate-like samples were corrected using a program DABEX[22]. The integrated intensities measured at equivalent indices were averaged. Number of independent reflections ($F>3\sigma(F)$) used for the structure determination is given in Table 1.

Standard crystal structure analysis was carried out using a least-square program RADIEL[22]. The atomic scattering factors and dispersion corrections were taken from *International Tables for Crystallography*[23]. Since both Sr^{2+} and Y^{3+} have 36 core electrons, their occupancy in crystal #1 cannot be practically determined from the diffraction intensities. Crystal #1 was thus analyzed assuming Sr-free at the Y-site. The Ca concentration of the other crystals was refined in the least-square calculation. The crystal structure of $Pb_2Sr_2Y_{1-x}Ca_xCu_3O_8$ was characterized by the oxygen disorder in the PbO planes[1]-[7]. Figure 2 shows the schematic representation of the possible oxygen sites in the crystals with the space groups, C2/m and Cmmm, respectively. Assuming such oxgen disorder in PbO planes, considerable reduction of the residuals (*R*-factors), R_F and R_{wF}, are achieved and their values are finally converged within the range of 0.058–0.077 as shown in Table 1. In the present calculation, fixed isotropic thermal parameter ($B=0.01$ nm^2) was assumed for the disordered oxygens in the four crystals. Table 2 presents obtained structural parameters. The crystal structure of $Pb_2Sr_2Y_{1-x}Ca_xCu_3O_8$ is schematically represented in Fig. 3. Interatomic distances between cations and the nearest neighbor oxygens are given in Table 3. There are some appreciable differences between the Pb–O(2) distances in the monoclinic and the orthorhombic crystals. The Cu(2)–O(3) chemical bondings form a two-dimensional CuO_2 network parallel to the *c*-plane. In the crystal #1 with $T_c=16.0$ K, there are two kinds of Cu(2)–O(3) bonds, namely, a short Cu(2)–O(3) bond (0.189(1) nm) and a long one (0.195(1) nm). In the crystals #2 ($T_c=64.8$ K), those bonds have the same distance within the experimental errors, though the space symmetry remains unchanged. The Cu(2)–Cu(2) distance parallel to the *c*-axis is plotted in Fig. 4 as a function of the Ca- or Sr-concentration, x, with ones obtained by Jorgensen and Andersen[8]. The interplaner distance between the PbO planes, Pb–Pb distance in Table 3, gradually in-

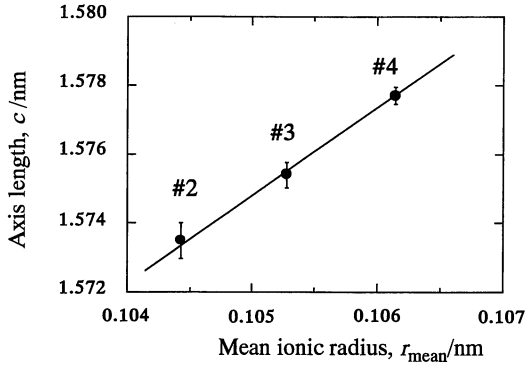

Fig. 1 *c*-axis length vs. mean ionic rudius r_{mean} at Ln site.

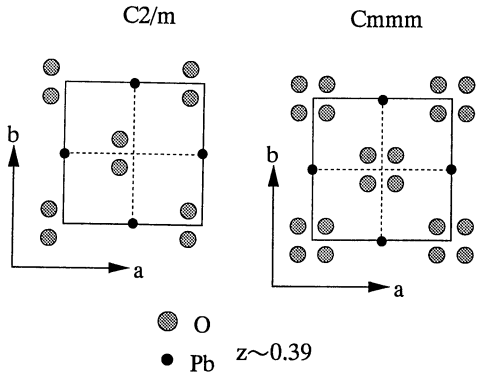

Fig. 2 Schematic representation of oxygen disorder in PbO plane for space groups, C2/m and Cmmm, respectively.

Table 2 Structural parameters of $Pb_2Sr_2Ln_{1-x}M_xCu_3O_8$. Equivalent thermal parameter was defined as B_{eq} (nm^2)=(8/3) $\pi^2\Sigma\Sigma U_{ij}$. Isotropic thermal parameter, B (nm^2), for O(2) was fixed.

		#1	#2		#3	#4
Pb	4*i* *x*	0.5005(2)	0.4974(2)	4*l* *x*	0	0
	y	0	0	*y*	0.5	0.5
	z	0.38769(7)	0.38734(6)	*z*	0.38718(8)	0.38684(6)
	B_{eq}	0.0060(4)	0.0078(3)	B_{eq}	0.0092(3)	0.0080(3)
Sr	4*i* *x*	−0.0002(4)	0.0044(4)	4*k* *x*	0	0
	y	0	0	*y*	0	0
	z	0.2208(2)	0.2200(1)	*z*	0.2195(1)	0.2197(2)
	B_{eq}	0.007(1)	0.008(1)	B_{eq}	0.0108(9)	0.0086(7)
Ln/M		Y/Sr	Y/Ca		Y/Ca	Ho/Ca
	occ.	1.0/0(fixed)	0.75(1)/0.25	*occ.*	0.59(2)/0.41	0.636(8)/0.364
	2*a* *x*	0	0	2*a* *x*	0	0
	y	0	0	*y*	0	0
	z	0	0	*z*	0	0
	B_{eq}	0.009(2)	0.007(2)	B_{eq}	0.007(2)	0.0042(7)
Cu(1)	2*c* *x*	0	0	2*d* *x*	0	0
	y	0	0	*y*	0	0
	z	0.5	0.5	*z*	0.5	0.5
	B_{eq}	0.008(3)	0.010(2)	B_{eq}	0.012(2)	0.012(2)
Cu(2)	4*i* *x*	0.5008(7)	0.5020(5)	4*k* *x*	0	0
	y	0	0	*y*	0	0
	z	0.1066(2)	0.1060(2)	*z*	0.1068(3)	0.1060(2)
	B_{eq}	0.006(2)	0.006(1)	B_{eq}	0.008(1)	0.0041(8)
O(1)	4*i* *x*	0.508(4)	0.500(4)	4*l* *x*	0.5	0.5
	y	0	0	*y*	0	0
	z	0.255(2)	0.253(1)	*z*	0.256(1)	0.252(1)
	B_{eq}	0.02(1)	0.02(1)	B_{eq}	0.007(6)	0.015(6)
O(2)	*occ.*	0.5	0.5	*occ.*	0.25	0.25
	8*j* *x*	−0.041(5)	0.048(4)	16*r* *x*	−0.046(7)	−0.068(11)
	y	−0.080(5)	−0.090(4)	*y*	−0.063(8)	−0.064(9)
	z	0.385(2)	0.386(1)	*z*	0.385(5)	0.382(4)
	B	0.01(fixed)	0.01(fixed)	*B*	0.01(fixed)	0.01(fixed)
O(3)	8*j* *x*	0.247(2)	0.251(2)	8*m* *x*	0.25	0.25
	y	0.253(2)	0.249(2)	*y*	0.25	0.25
	z	0.0947(8)	0.0937(7)	*z*	0.095(1)	0.0948(7)
	B_{eq}	0.009(11)	0.011(9)	B_{eq}	0.012(6)	0.009(5)

creases with decreasing the area of *c*-plane.

2. Bond-valence sum calculation

Table 4 shows cation valence, v_i, of Pb, Sr, Cu(1) and

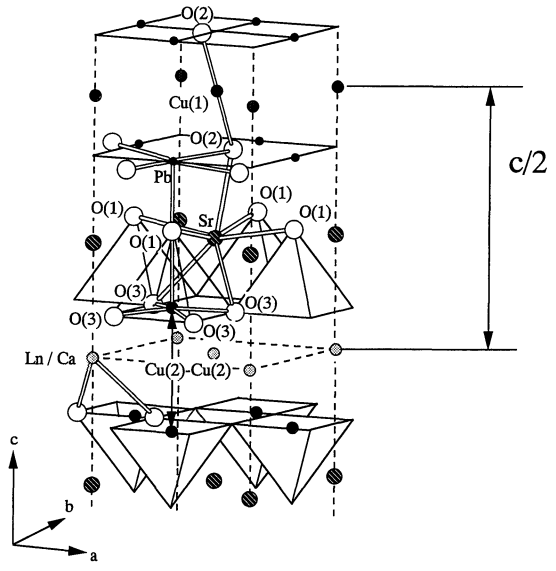

Fig. 3 Partly represented crystal structure of $Pb_2Sr_2Ln_{1-x}M_xCu_3O_8$.

Table 3 Interatomic distances (nm) between cation and nearest-neighbor oxygens, interplaner distances, Cu(2)-Cu(2)(nm), Pb-Pb(nm) and $a\times b$ cross-section area of unit cell (nm^2).

		#1	#2	#3	#4
Pb-O(1)	×1	0.209(3)	0.212(2)	0.207(2)	0.212(2)
Pb-O(2)	×1	0.251(3)	0.247(2)	0.247(4)	0.235(6)
	×1	0.295(3)	0.300(2)	0.296(4)	0.308(6)
	×1	0.229(3)	0.224(2)	0.237(4)	0.238(5)
	×1	0.316(3)	0.321(2)	0.305(4)	0.307(5)
Sr-O(3)	×2	0.276(1)	0.276(1)	0.274(1)	0.2737(8)
	×2	0.276(1)	0.275(1)	0.274	0.2737
Sr-O(1)	×2	0.2768(5)	0.2760(3)	0.2758(4)	0.2742(4)
	×1	0.270(2)	0.272(2)	0.2759(4)	0.2746(4)
	×1	0.279(2)	0.276(2)	0.2759	0.2746
Sr-O(2)	×1	0.263(2)	0.261(2)	0.264(7)	0.262(6)
Ln-O(3)	×4	0.243(1)	0.242(1)	0.2427(10)	0.2422(7)
	×4	0.242(1)	0.241(1)	0.2427	0.2422
Cu(1)-O(2)	×2	0.188(3)	0.193(2)	0.186(7)	0.192(6)
Cu(2)-O(3)	×2	0.189(1)	0.192(1)	0.198(2)	0.194(1)
	×2	0.195(1)	0.192(1)	0.198	0.194
Cu(2)-O(1)	×1	0.233(3)	0.231(2)	0.235(2)	0.231(2)
Cu(2)-Cu(2)		0.3355(3)	0.3336(5)	0.3370(4)	0.3340(3)
Pb-Pb		0.3534(2)	0.3545(2)	0.3560(1)	0.3565(1)
$a\times b$		0.2928(1)	0.2917(7)	0.2914(1)	0.29056(1)

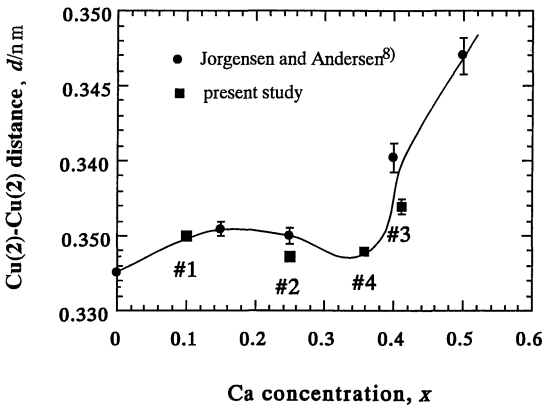

Fig. 4 Cu(2)-Cu(2) distance vs. divalent-cation concentration x. The present results are denoted with filled squares. Filled circles were obtained by Jorgensen and Andersen[8]. Solid line is a guide for the eyes.

Table 4 Cation valence obtained by the bond-valence sum calculation.

	#1(x=0.10)	#2(x=0.25)	#3(x=0.41)	#4(x=0.36)
Pb^{2+}	2.2(2)	2.2(1)	2.2(2)	2.1(2)
Sr^{2+}	1.67(4)	1.70(4)	1.70(3)	1.74(2)
$Cu(1)^{1+}$	1.16(9)	1.01(5)	1.2(3)	1.0(2)
$Cu(2)^{2+}$	2.26(7)	2.26(7)	2.26(2)	2.30(1)
Ln^{3+}/M^{2+}	Y^{3+}/Sr^{2+} 2.74(7)	Y^{3+}/Ca^{2+} 2.65(7)	Y^{3+}/Ca^{2+} 2.50(7)	Ho^{3+}/Ca^{2+} 2.58(5)

Cu(2) estimated from the following bond-valence sum equation[24]:

$$v_i=\sum \exp[(r_0-r_{ij})/0.37], \quad (9)$$

where r_0 is an empirically determined parameter for each cation-oxygen bond and r_{ij} is a distance between the i-th cation and the j-th coordinating oxygen. The cation valences for Pb and Cu(1), being 2+ and 1+, respectively, are practically constant for all crystals, but, for the Sr and Cu(2), somewhat larger than the formula value 2+ in the crystal #4 having the highest T_c. The valence for partly substituted lanthanide was also calculated assuming the observed value of r_0 for Y^{3+} (or Ho^{3+}) and the doped divalent cation, being monotonically decreasing with increasing nominal hole carrier concentration.

3. Electron density map by MEM

The unit cell was devided into $N_p=64\times64\times128$ partial volumes (pixels) and the initial density of every pixels was set to $N_e/(N_p\times V)$, where V is the unit cell volume and N_e is total number of electrons in a unit cell, which was deduced from the formal ionic valences (Table 5). The structure factors were normalized to the electron unit from the observed Bragg intensities. The phase term for each structure factor was determined at the final stage of the least square calculation. The electron density was calculated in the region of minimum asymmetric unit, $0\leqq x\leqq 1/2$, $0\leqq y\leqq 1/4$, $0\leqq z\leqq 1$ for C2/m and $0\leqq x\leqq 1/4$, $0\leqq y\leqq 1/2$, $0\leqq z\leqq 1/2$ for Cmmm[25], respectively. The whole electron distribution maps in the unit cells were obtained by the symmetry operations. We chose $\lambda=0.2$ as the Lagrange multiplier through this study, since the fastest convergence was realized with this value in the test calculation for rutile. It is known that the electron density distribution obtained by the MEM do not depend (if the calculation will be successfully converged) on a choice of the λ value[26]. The convergence criterion, $C\leqq 1$, was successfully reached for crystals #1, #2, #3 and #4 after 650, 493, 688 and 550 iteration cycles, respectively. The final residuals (R-factors) are slightly smaller than those in the least-square calculation. In the crystal #4, unidentified electron density peaks were found in the vicinity of heavy ions, Ho^{3+} and Pb^{2+}. The smallest residuals for this crystal are probably caused by those spurious peaks. For this reason, the crystal #4 was excluded from the comparison of the electron density maps.

Figure 5 shows the electron density maps of the PbO

Table 5 Total number of electrons in unit cell and residuals (R-factors) in MEM calculation.

	#1	#2	#3	#4
N_e	860	850.71	845.05	882.59
R_F	0.060	0.049	0.055	0.033
R_{wF}	0.067	0.050	0.065	0.039

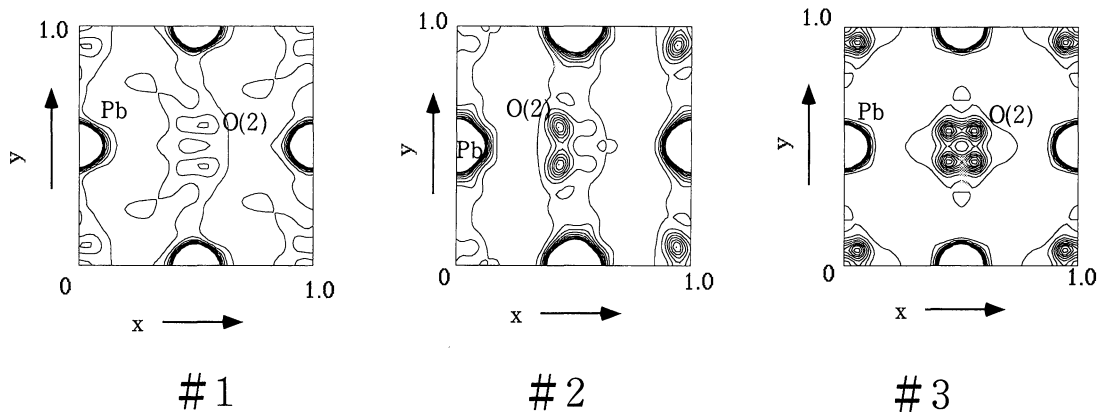

Fig. 5 Electron density maps of PbO_2 plane with 1×10^3 e/nm^3 contour steps in the range of $(0\text{-}1)\times10^4$ e/nm^3.

plane at z=0.39. The rather coase contour step of 1×10^3 e/nm^3 was used to avoid complication. The O(2) ion splits into two positions in the monoclinic crystals (#1 and #2) and into four positions in the orthorhombic ones (#3), respectively. Peak splitting for the O(2) ion is consistent with the oxygen disorder models (Fig. 2) introduced

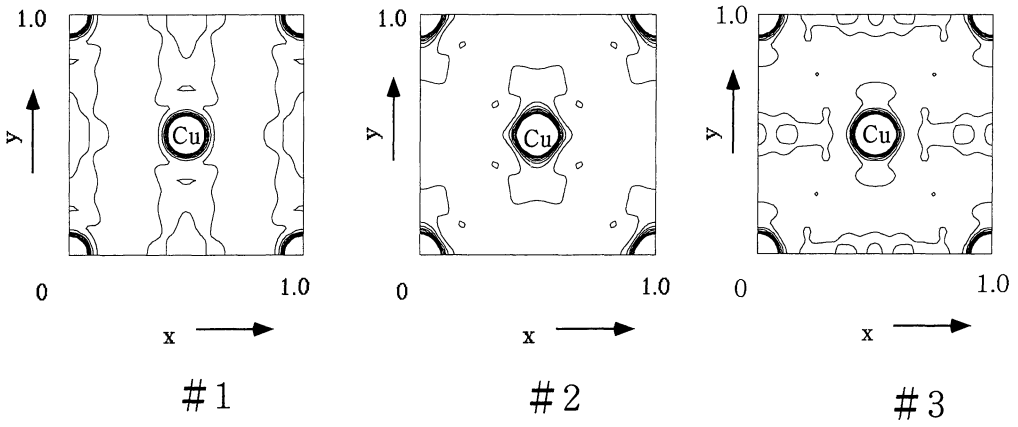

Fig. 6 Electron density maps of monovalent Cu layer with 1×10^3 e/nm^3 contour steps in the range of (0–1)$\times10^4$ e/nm^3.

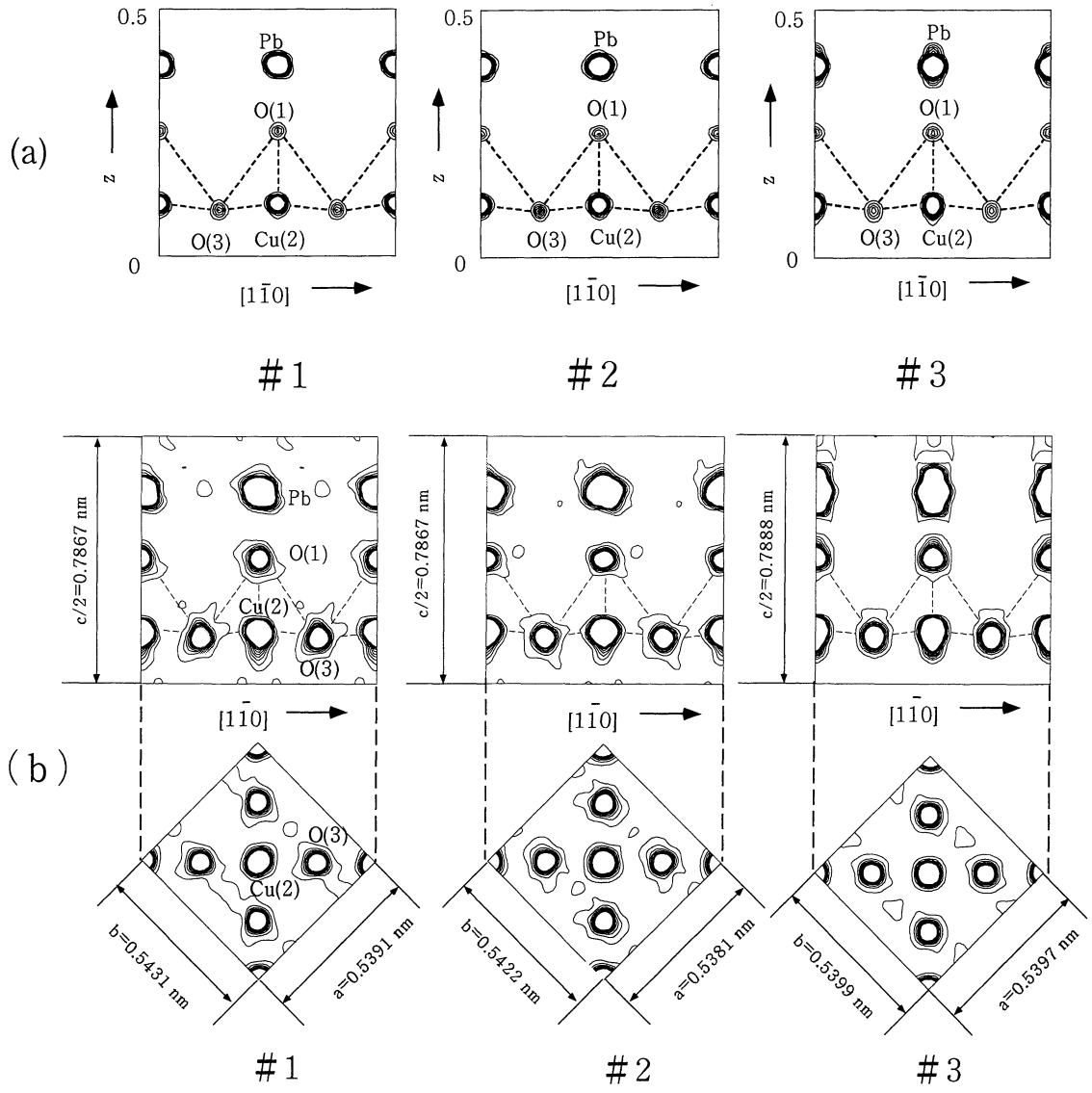

Fig. 7 (a) Electron density maps of a plane containing Pb, O(1), O(3) and Cu(2) ions (a) in the range of (0–1)$\times10^5$ e/nm^3 with 1×10^4 e/nm^3 contour steps and (b) in (0–1)$\times10^4$ e/nm^3 with 1×10^3 e/nm^3 steps. (b) includes the CuO_2 plane at z=0.095 ($0.5\leqq x\leqq1.5$, $0\leqq y\leqq1.0$).

to the present structure determination, though the O(2) peaks of the crystal #1 are much lower than those of the other crystals. It seems that, in crystal #2, the Pb ion is weakly linked to O(2) ion parallel to the [010] direction. The electron density maps of $a \times b$ plane at $z=0.5$ is shown in Fig. 6. The Cu(1) ions are clearly found at the positions of (0, 0, 1/2) and (1/2, 1/2, 1/2), where some low and extended distribution parallel to the [010] direction is seen in the vicinity of Cu(1) ion. If excess oxygens might be absorbed into this plane during the crystal growth, those atoms may situate in the particular plane. But, there is no extra sharp peak corresponding to the excess oxygen, indicating that annealing in pure N_2 gas was properly done.

In the 3212-type lead cuplates, there is a plane containing the Pb, Cu(2), O(3) and O(1) ions parallel to (110) plane. Figure 7(a) and (b) show the electron density distribution in this plane ($0 \leqq z \leqq 1/2$), (a) the coarsely contoured maps of $(0\text{–}1) \times 10^5$ e/nm^3 region with 1×10^4 e/nm^3 steps, (b) the finely contoured maps of $(0\text{–}1) \times 10^4$ e/nm^3 region with 1×10^3 e/nm^3 steps, respectively. In addition to those maps, Fig.7(b) contains the electron density map of the CuO_2 plane. Broken lines correspond to the O–O and Cu–O bonds in CuO_5 pyramids. One can see remarkably anisotropic electron density distributions for the Pb ion in crystal #3, relative to crystals #1 and #2. In crystal #3, the electron density distribution of the apical O(1) and O(3) is also anisotropic as shown in Fig. 7(b). The Cu(2) ions exhibit somehow anomalous distributions normal to the CuO_2 plane in all three crystals.

IV. Discussion

1. Cu^{2+} and Cu^{1+} ions

The electron density distribution in tetragonal $YBa_2Cu_3O_{6+\delta}$ ($\delta=0.38$) was studied in detail by the difference-Fourier synthesis[27]. A pair of positive peaks, an indication of the $3d_{z^2}$ orbital, were found at the distance of 0.092 nm from the in-plane Cu(2) position along the [001] direction, while no residual electron density was observed around the Cu^{1+} in the chain structure, corresponding to a spherical distribution of $3d^{10}$ electrons. The 3212-type lead cuprates also have two kinds of Cu ions similar to the $YBa_2Cu_3O_{6+\delta}$. In the present study, the elongated electron density distribution along the direction normal to the CuO_2 plane is shown in the vicinity of Cu(2) ion. However, no counterpart was observed in the opposite direction toward the apical oxygen. At present, it is not certain whether this $3d_{z^2}$-like distribution is real or not. In contrast, the Cu(1) ion has a spherical electron density distribution, suggesting that the Cu(1) ion is in the monovalent state with fully occupied $3d^{10}$ electronic configuration. This is consistent with the bond valence sum calculation in Table 5.

2. Pb^{2+} ion

The $(6s)^2$ electrons of Pb^{2+} ion are localized far from the core electrons and do not participate in a chemical bonding to the other ions. They are called lone pair or inert pair, which causes the stereochemical activity of Pb^{2+} ion in several lead oxides[28]-[32]. In the Pb-3212 type compound, it is natural to consider that the lone pair occupies open space between Cu^{1+} layer and PbO plane. In order to explain the oxygen disorder in the orthorhombic $Pb_2Sr_2YCu_3O_8$, Cava *et al.*[2] postulated that the lone pair orbital is randomly oriented roughly normal to one of (114), ($1\bar{1}4$) and their equivalent planes. Xue *et al.*[21] indicated that the same postulation can be applied to the monoclinic 3212-type compounds. In this study, we found that the PbO interplaner distance gradually increases with decreasing $a \times b$ cross section area. The following is conceivable for our observation based on their posturation. In the contraction of $a \times b$ cross-section, the lone pair orbitals are oriented close to the *c*-direction by their Coulomb repulsion in the $a \times b$ plane. The repulsion force along the *c*-direction grows strong between the upper and lower PbO planes, so that the PbO interplaner distance increases.

The electron cloud of the Pb^{2+} ion spreads almost isotropically in crystals #1 and #2, but anisotropically in the crystal #3. It is not appropriate to interprete this vertically elongated distribution due to the anisotropic thermal vibrations of Pb^{2+} ion, since the core electrons of the Pb^{2+} ion in crystal #3 are isotropic as shown in Fig. 7(a). Anomalously shaped electron density distribution is sometimes associated with the local and almost random displacements of ions. However, such displacements of Pb^{2+} ions are unlikely to occur along the *c*-direction because of the short. Pb–O(1) distance (0.207(2) nm) and the repulsion between the Pb^{2+} ion pairs. At present, we cannot relate the anomalous electron cloud of the Pb^{2+} ion with any particular cause.

3. Oxygens in CuO_2 plane

The electron density distribution of in-plane oxygen, O(3), is vertically elongated in the crystal #3, while irregularly skewed in crystals #1 and #2. This is possibly related to changes of the O(3) thermal vibration by the Ca-doping. Currat *et al.*[33] found that the phonon density of states of $Pb_2Sr_2Y_{0.5}Ca_{0.5}Cu_3O_8$ considerably increases in the energy regions of 30–40 and 60–75 meV at 300 K, relative to non-doped $Pb_2Sr_2YCu_3O_8$. The lower energy region includes two zone center optic phonon modes, *i.e.*, in-phase Sr–O(3) motion (A_{1g}) and a B_{2u} silent mode comprising only O(3) vibration[33][34]. In both modes, the O(3) has the displacement vector parallel to the *c*-direction. In $Pb_2Sr_2Y_{0.75}Ca_{0.25}Cu_3O_8$, the A_{1g} symmetry mode was assigned to a peak at 240 cm^{-1} (30 meV) by Raman scattering measurement[35]. However, the large thermal amplitude of O(3) is not necessarily ascribed to the above phonon modes because their phonon branches can be highly dispersive when going away from the Brillouin zone center. Another possibility is the tilting motion of CuO_5 pyramid around the [100] and [010] axes passing through the Cu(2) ion, such as the CuO_6 octahedron rotational mode in orthorhombic La_2NiO_4[36]. This idea arises from the horizontally expanded electron cloud of the api-

cal O(3) in crystal #3.

V. Conclusions

The high-T_c superconductors, $Pb_2Sr_2Y_{0.90}Sr_{0.10}Cu_3O_8$, $Pb_2Sr_2Y_{1-x}Ca_xCu_3O_8$ (x=0.25 and 0.41) and $Pb_2Sr_2Ho_{0.64}Ca_{0.36}Cu_3O_8$, were studied by means of single crystal X-ray diffraction technique. These compounds exhibit structural change from the monoclinic crystal to the orthorhombic one with increasing the divalent cation concentration. Their crystal structures were successfully determined assuming the space groups, C2/m (x=0.10 and 0.25) and Cmmm (x=0.36 and 0.41), respectively. The bond-valence sum for the cations was calculated based on the obtained positional parameters.

Detailed electron density distributions of $Pb_2Sr_2Y_{0.90}Sr_{0.10}Cu_3O_8$ and $Pb_2Sr_2Y_{1-x}Ca_xCu_3O_8$ (x=0.25 and 0.41) are obtained by applying the MEM, while the phases of the observed structure factors are fixed at the values constraint with the structure model. The summary of the results is shown below.

(1) There is no excess oxygen in the monovalent copper layer of any crystals. This is consistent with the present bond valence sum calculation for the Cu^{1+} ion.

(2) The oxygens in the PbO plane split into four sites in orthorhombic, but two sites in monoclinic crystals, which agrees with the structure determination.

(3) The feature common to the present crystals is the anomalous electron density distribution of the Cu(2) ion. This may be related to mixed valency of the Cu(2) due to the charge transfer from the Y/Ca plane.

(4) The electron cloud of Pb^{2+} ion is highly anisotropic in the orthorhombic crystal with x=0.41, which can be interpreted in term of neither the anisotropic thermal vibration nor the local and almost random displacements of the Pb^{2+} ion.

(5) The electron density distribution of O(3) is elongated parallel to the c-direction in the orthorhombic crystal (x=0.41), which corresponds to the increase of the phonon density of states in $Pb_2Sr_2Y_{0.5}Ca_{0.5}Cu_3O_8$. There are two possible origins. One is the zone center modes, the in-phase Sr–O(3) motion (A_{1g}) and the B_{2u} silent mode comprising only O(3) vibration. The other is the tilting motion of CuO_5 pyramid. In order to clarify the relation between the thermal motion of oxygens and the superconductivity, it is desirable to study the electron density distribution of $Pb_2Sr_2Y_{1-x}Ca_xCu_3O_8$ in the low temperature range including T_c.

Acknowledgment

This work was partly supported by a Grant-in-Aid for Scientific Research from the Ministry of Education, Science, Sports and Culture of Japan.

REFERENCES

(1) R. J. Cava, B. Batlogg, J. J. Krajewski, L. W. Rupp, L. F. Schneemeyer, T. Siegrist, R. B. van Dover, P. Marsh, W. F. Peck, Jr., P. K. Gallagher, S.H. Glarum, J. H. Marshall, R. C. Farrow, J. V. Waszczak, R, Hull and P. Trevor:Nature, **336** (1988), 211.
(2) M. A. Subramanian, J. Gopalakrishnan, C. C. Trardi, P. L. Gai, E. D. Boyes, T. R. Askew, R. B. Flippen, W. E. Farneth and A. W. Sleight: Physica, **C157** (1989), 124.
(3) H. Fujishita, S. Yamagata and M. Sato: J. Phys. Soc. Jpn., **60** (1991), 913.
(4) T. Mochiku and K. Kadowaki: J. Phys. Soc. Jpn., **61** (1992), 881.
(5) O. Chmaissen, C. Chaillout, J. J. Capponi, M. Marezio and J. L. Tholence:J. Alloys and Compounds, **195** (1993), 169.
(6) R. J. Cava, M. Marezio, J. J. Krajewski and W. F. Peck Jr., A. Santro and F. Beech: Physica, **C157** (1989), 272.
(7) C. Chaliout, O. Chmaissen, J. J. Capponi, T. Fournier, G. J. McIntyre and M. Marezio: Physica, **C175** (1991), 293.
(8) J. E. Jorgensen and N. H. Andersen: Physica, **C218** (1993), 43.
(9) H. Fujishita, M. Sato, Y. Morii and S. Funahashi: Physica, **C210** (1993), 529.
(10) H. W. Zandbergen, K. Kadowaki, M. J. V. Menken, A. A. Menovsky, G. Van. Tendeloo and S. Amelinckx: Physica, **C158** (1989), 155.
(11) E. A. Hewat, J. J. Capponi, R. J. Cava, C. Chaillout, M. Marezio and J. L. Tholence: Physica, **C157** (1989), 509.
(12) D. M. Collins: Nature, **298** (1982), 49.
(13) M. Sakata, R. Mori, S. Kumazawa and M. Takata: J. Appl. Cryst., **23** (1990), 526.
(14) M. Sakata, T. Uno, M. Takata and R. Mori: Acta Crystallogr., **B48** (1992), 591.
(15) M. Masuzawa, T. Noji, Y. Koike and Y. Saito: Jpn. J. Appl. Phys., **28** (1989), L1524.
(16) T. Noji, Y. Koike, K. Ohtsubo, S. Shiga, M. Kato, A. Fujiwara and Y. Saito: Jpn. J. Appl. Phys., **33** (1994), 2515.
(17) T. Noji, T. Takabayashi, M. Kato, T. Nishizaki, N. Kobayashi and Y. Koike: Physica, **C225** (1995), 10.
(18) A. Khachaturyan and S. Semonovskaya and B. Vainshtein: Acta Crystallgr., **A37** (1981), 742.
(19) R. Narayan and R. Nityananda: Acta Crystallgr., **A38** (1982), 122.
(20) R. D. Shanon and C. T. Prewitt: Acta. Cryst., **B25** (1969), 925.
(21) J. X. Xue, J. E. Greedan and M. Maric: J. Solid State Chem., **102** (1993), 501.
(22) P. Coppens, T. N. Gurutov, P. Leung, E. D. Stevens, P. D. Becker and Y. W. Yang: Acta Crystallogr., **A35** (1979), 63.
(23) *International Tables for Crystallography*, ed. by T. Hahn, D. Reidel Publishing Co., Dordrecht, Vol. A, (1983), p. 158 and 294.
(24) I. D. Brown and D. Altermatt: Acta. Crystallogr., **B41** (1985), 244.
(25) *International Tables for X-ray Crystallography*, ed. by J. A. Ibers and W. C. Hamilton, The Kynoch press, Birmingham, Vol. IV, (1974), p. 71.
(26) M. Sakata and M. Sato: Acta Crystallogr., **A46** (1990), 263.
(27) S. Sasaki, Z.Inoue, N. Iyi and S. Takekawa: Acta Crystallogr., **B48** (1992), 393.
(28) W. T. Fu, H. W. Zandbergen, W. G. Haije and L. J. De Jongh: Physica, **C159** (1989), 210.
(29) T. Rouillon, J. Provost, M. Hervieu, D. Groult, C. Michel and B. Raveau: Physica, **C159** (1989), 201.
(30) T. Rouillon, V. Caignaert, C. Michel, M. Hervieu, D. Groult and B. Raveau: J. Solid State Chem., **97** (1992), 19.
(31) T. Rouillon, M. Hervieu, B. Domenges and B. Raveau: J. Solid State Chem., **103** (1993), 63.
(32) D. Le. Bellac, J. M. Kiat and P. Garnier: J. Solid State Chem., **114** (1995), 459.
(33) R. Currat, A. J. Dianoux, P. Monceau and J. J. Capponi: Phys. Rev., **B40** (1989), 11362.
(34) W. Kress, J. Prade, U. Schroder, A. D. Kulkarni and F. W. de Wette: Physica, **C162-164** (1989), 1345.
(35) Ran Liu, M. Cardona, B. Gegenheimer, E. T. Heyen and C. Thomsen: Phys. Rev., **B40** (1989), 2654.
(36) G. Burns, F. H. Dacol, D. E. Rice, D. J. Buttrey and M. K. Crawford: Phys. Rev., **B42** (1990), 10777.